[redacted]

AEC RESEARCH AND DEVELOPMENT REPORT

ORNL-2442 cy. 77A
C-84 - Reactors - Special Features of Aircraft Reactors
M-3679 (20th ed., Rev.)

THERMAL STRESS ANALYSIS OF THE ART HEAT EXCHANGER CHANNELS AND HEADER PIPES

D. L. Platus

OAK RIDGE NATIONAL LABORATORY
operated by
UNION CARBIDE CORPORATION
for the
U.S. ATOMIC ENERGY COMMISSION

[redacted]

[redacted]

ORNL-2442
C-84 - Reactors - Special Features
of Aircraft Reactors
M-3679 (20th ed., Rev.)

This document consists of 38 pages.
Copy 77 of 227 copies. Series A.

Contract No. W-7405-eng-26

REACTOR PROJECTS DIVISION

THERMAL STRESS ANALYSIS OF THE ART HEAT EXCHANGER CHANNELS AND HEADER PIPES

D. L. Platus

DATE ISSUED

MAR 4 1958

OAK RIDGE NATIONAL LABORATORY
Oak Ridge, Tennessee
operated by
UNION CARBIDE CORPORATION
for the
U.S. ATOMIC ENERGY COMMISSION

[redacted]

[redacted]

NOMENCLATURE

Subscripts on Deflections:

P	deflections due to in-plane bending of channel
N	deflection due to out-of-plane bending of channel
r	deflection due to rigid-body rotation of plane of channel about y-axis
T	deflections due to relative thermal expansion of channel
H	deflections due to deformations of header pipe

Symbols:

x, y, z	rectangular coordinates
x_b, z_b	coordinates of point b
$\overline{ob}$	distance from origin to point b
ϕ	angle between negative x-axis and $\overline{ob}$
r	radius of curve of channel
r_H	maximum radius of header pipe
ℓ	length of header pipe
p, n	directions in xz-plane, parallel and normal to plane of curve, respectively
$\delta x, \delta y, \delta z$	deflections parallel to x-, y-, and z- axes, respectively
δp, δn	deflections in plane and normal to plane of curve, respectively
$\delta\theta$, $\delta\phi$, $\delta\gamma$	angular deflections with rotation vectors parallel to x-, y-, and z- axes, respectively
$\delta\psi_p, \delta\psi_n$	angular deflections with rotation vectors parallel to p and n, respectively
F_x, F_z	forces parallel to x- and z- axes, respectively

[redacted]

[redacted]

P, N forces parallel to p and n, respectively

M_x, M_y, M_z moments parallel to x-, y-, and z- axes, respectively

M_P, M_N moments parallel to p and n, respectively

M_t, M_r, M_n moments tangent, radial, and normal to plane of curve at equator, respectively

M_H resultant bending moment acting on header pipe

M_{Hx}, M_{Hy} x- and y- components of M_H

$\sigma, \sigma_1, \sigma_2$ normal stresses

σ_N, σ_n stresses due to in-plane bending of channel

σ_P, σ_r stresses due to out-of-plane bending of channel

τ shear stress or twisting stress

C a function of the cross section used in calculating shear stress

K a function of the cross section used in calculating torsional rigidity

I_P moment of inertia of channel cross section about an axis radial to the curve

I_N moment of inertia of channel cross section about an axis normal to plane of curve

Z_P section modulus of channel about an axis radial to the curve

Z_N section modulus of the channel about an axis normal to the curve

I_H moment of inertia of cross section of header pipe

J_H polar moment of inertia of cross section of header pipe

ν poisson's ratio

E modulus of elasticity

G shear modulus, $G = \dfrac{E}{2(1 + \nu)}$

$a_{11}, a_{12}, \text{---} a_{66}$ coefficients in set of linear algebraic equations

α linear coefficient of expansion; angle describing direction of M_H

T temperature

[redacted]

[redacted]

THERMAL STRESS ANALYSIS OF THE ART HEAT EXCHANGER CHANNELS AND HEADER PIPES

This report summarizes the study which was made to determine the stresses, deflections, and the forces and moments acting on the ART heat exchanger channels and header pipes due to relative thermal expansion between the channels and the pressure shell at full power operation.

Introduction

Figure 1 shows a sketch of a channel and header pipes, and a portion of the pressure shell to which they are connected. During full power operation the temperature of the channel will be higher than that of the pressure shell, and thereby produce relative thermal expansion. The resulting forces and moments will cause deformation of the channel, the header pipes, and the thermal sleeves which connect the pipes to the pressure shell. The stresses due to these loads will be transmitted to the incoming NaK piping.

Figure 2 shows the idealized system used for the analysis. The channel was treated as a semi-circular-arc curved-beam connected directly to the header pipes, which were treated as cantilever beams. This analysis assumes that there is no deformation in the incoming NaK piping, or in the thermal sleeves. It is expected that this assumption will yield an adequate initial estimate for the analysis of the channel.

Because of symmetry it was sufficient to consider only one-half of the channel and one header pipe. The channel was assumed fixed at the mid-point and the deflections due to the relative thermal expansion were applied to the system. Elastic theory was assumed for all calculations.

[redacted]

[redacted]

FIG. 1 - SKETCH OF CHANNEL, HEADER PIPES AND ORIENTATION IN REACTOR

[redacted]

ORNL-LR-DWG. 27494

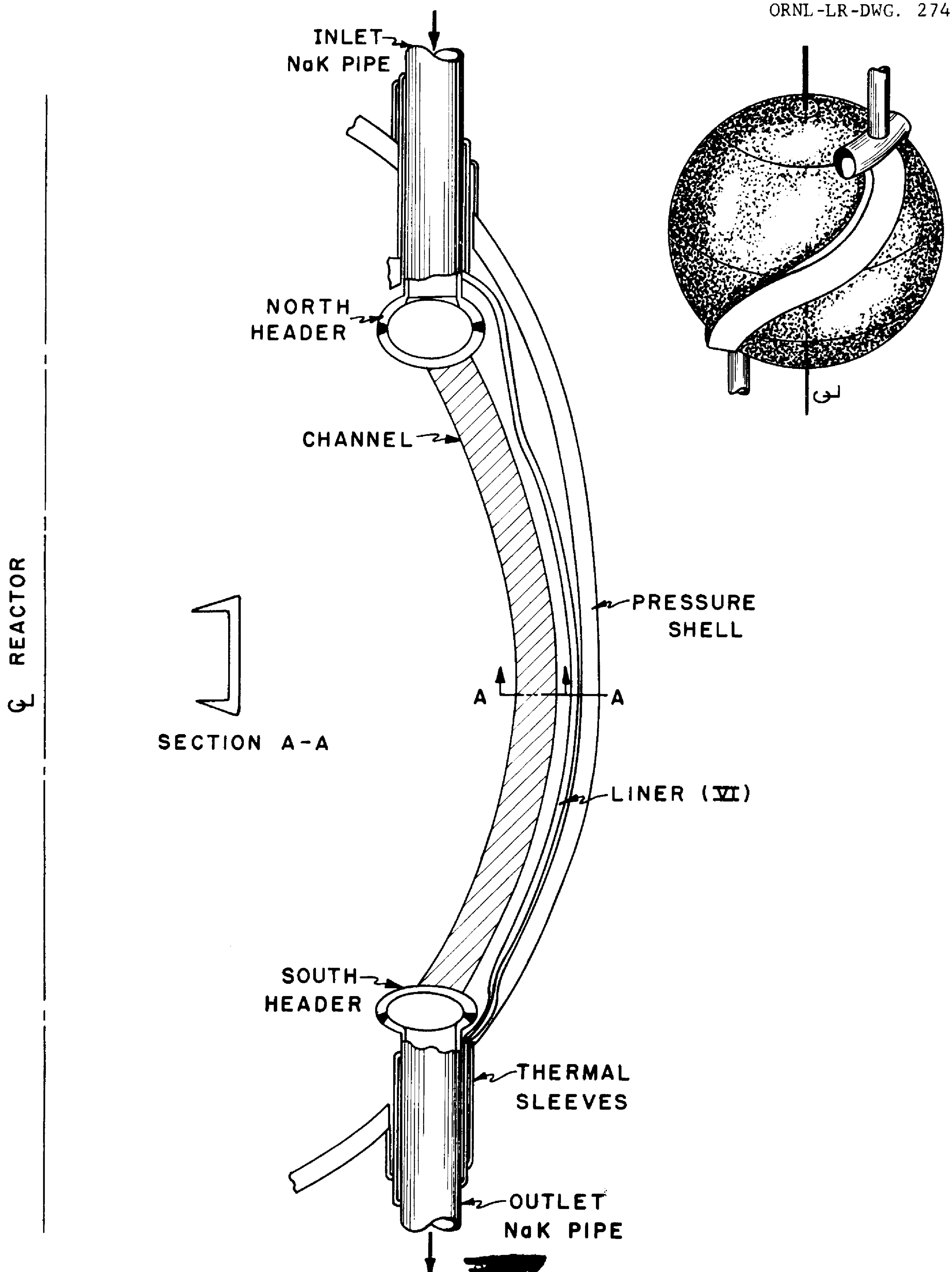

[redacted]

[redacted]

[redacted]

ORNL-LR-DWG. 27495

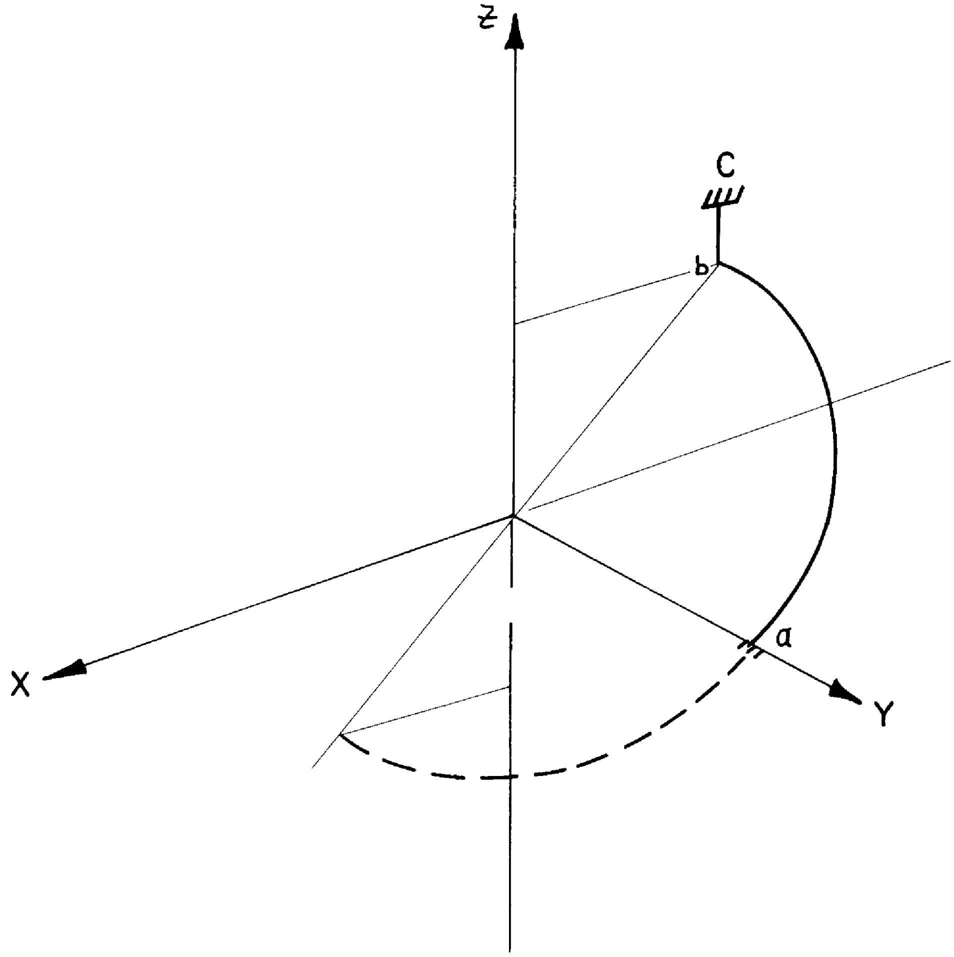

FIG. 2 — SKETCH BEAM STRUCTURE USED TO APPROXIMATE CHANNEL AND HEADERS

[redacted]

[redacted]

Thermal Expansions

The total vertical expansion of the channel relative to the pressure shell was reported in ART Design Memo 8-D-5 as 82 mils. This was assumed to be distributed equally between the sections above and below the mid-point, so that 41 mils was the vertical deflection used in the calculations.

For the radial expansion, the channel was assumed to be at an average temperature of 1425°F and the pressure shell at 1240°F. Taking the radial position of the header pipes to be 19.59 inches, this gives a radial deflection of 32 mils.

Method of Analysis

Deflection equations were written to determine the forces and moments acting on the channel at point b, from the thermal expansions applied between points a and c. The coordinate system is shown in Fig. 3. Since the channel is free to grow radially, forces were not applied in the y-direction. The modes of deformation included in-plane and out-of-plane bending of the channel from flexure and torsion and deformation of the header pipe by flexure and torsion.

The deflections for point b due to deformation and rotation of the channel may be expressed by the following equations, in which the subscripts refer to the modes of deflection.

$$\delta x = \delta x_P + \delta x_N + \delta x_r \tag{1}$$

$$\delta z = \delta z_P + \delta z_N + \delta z_r \tag{2}$$

$$\delta \theta = \delta \theta_P + \delta \theta_N \tag{3}$$

$$\delta \phi = \delta \phi_N + \delta \phi_r \tag{4}$$

$$\delta \gamma = \delta \gamma_P + \delta \gamma_N \tag{5}$$

[redacted]

[redacted]

[redacted]

ORNL-LR-DWG. 27496

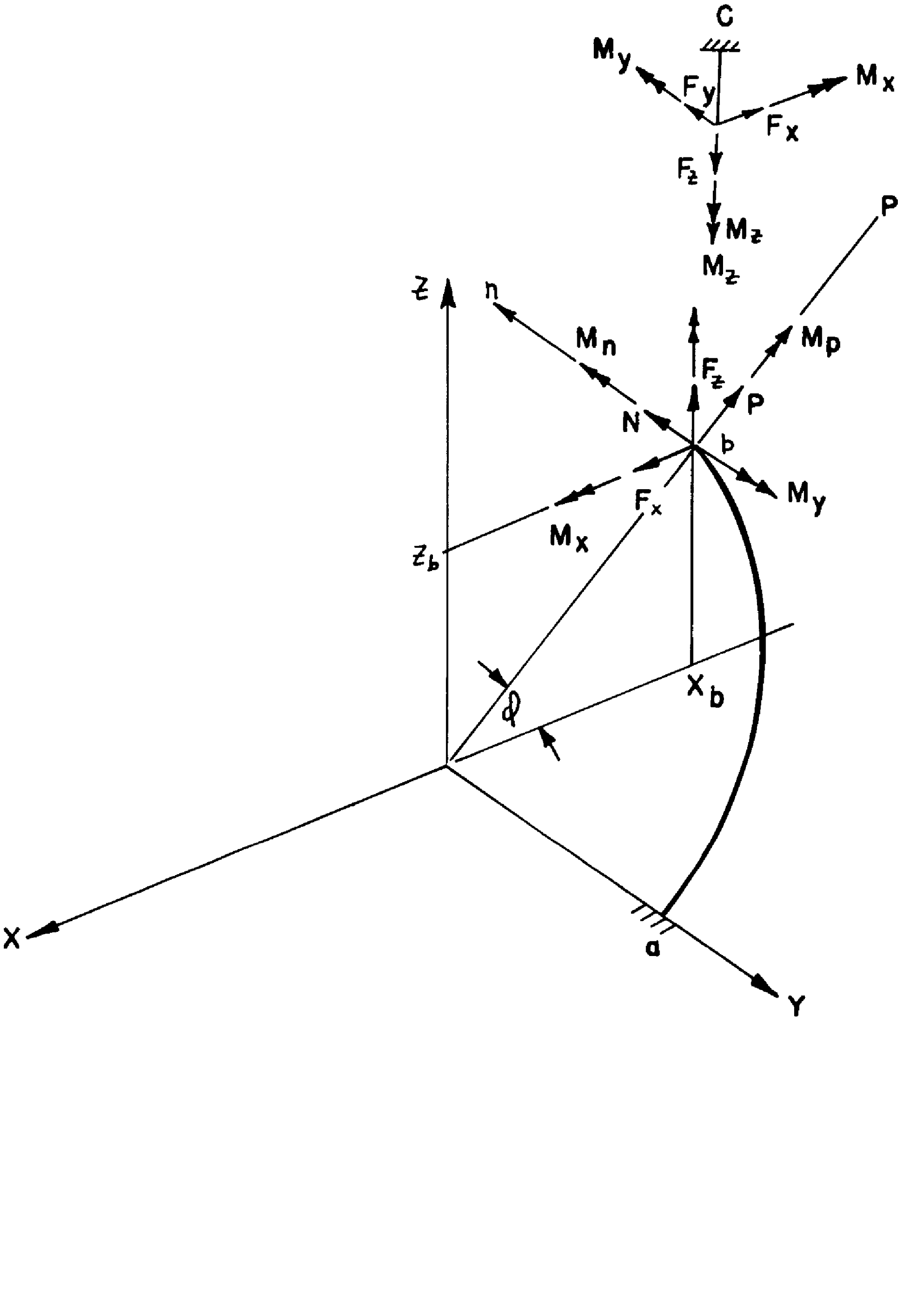

FIG. 3 – COORDINATE SYSTEM SHOWING FORCES AND MOMENTS ACTING ON CHANNEL AND HEADER PIPE

[redacted]

[redacted]

The relative thermal expansions applied between points a and c must be equal to the differences in the deflections of point b caused by deformations of the channel and those caused by deformations of the header pipe. Hence, the following relations may be written, in which the subscripts T and H refer to the applied relative thermal expansions and the deflections due to deformation of the header pipe, respectively[1].

$$\delta x_P + \delta x_N + \delta x_r - \delta x_H = \delta x_T \tag{6}$$

$$\delta z_P + \delta z_N + \delta x_r = - \delta z_T \tag{7}$$

$$\delta \theta_P + \delta \theta_N - \delta \theta_H = 0 \tag{8}$$

$$\delta \phi_N + \delta \phi_r - \delta \phi_H = 0 \tag{9}$$

$$\delta \gamma_P + \delta \gamma_N - \delta \gamma_H = 0 \tag{10}$$

By expressing the deflections in Eqs (6) through (10) in terms of the loads acting on the channel at point b, a set of equations results from which these loads may be determined. Since the rigid body rotation of the plane of the channel about the y-axis is an unknown in addition to the five loads F_x, F_z, M_x, M_y and M_z, an additional equation is required, and may be written by summing moments about the y-axis.

$$\Sigma M_y = M_y + F_x z_b - F_z x_b = 0 \tag{11}$$

<u>Deflections From In-Plane Bending of Channel</u>

It is seen from Fig. 3, that the force and moment producing in-plane bending of the channel are P and M_N. These may be resolved into forces and moments parallel to the coordinate axes.

$$P = F_z \sin \phi - F_x \cos \phi \tag{12}$$

$$M_N = M_x \sin \phi + M_z \cos \phi \tag{13}$$

1. The applied relative thermal expansions are taken as positive for both the x and z directions. Note also that the deformation of the header pipe in the z direction has been neglected.

[redacted]

The deflections due to these loads with respect to the p- and n- axes are given by[2]

$$\delta_p = \frac{\pi}{4}\,\frac{Pr^3}{EI_N} - \frac{M_N r^2}{EI_N} \tag{14}$$

$$\delta\psi_n = -\frac{Pr^2}{EI_N} + \frac{\pi}{2}\,\frac{M_N r}{EI_N} \tag{15}$$

Resolving these deflections into components along the coordinate axes,

$$\delta x_p = -\delta p \cos\phi \tag{16}$$

$$\delta z_p = \delta p \sin\phi \tag{17}$$

$$\delta\theta_p = \delta\psi_n \sin\phi \tag{18}$$

$$\delta\gamma_p = \delta\psi_n \cos\phi \tag{19}$$

Substituting Eqs (12) through (15) into Eqs (16) through (18),

$$\begin{aligned}\delta x_p = {} & \frac{\pi}{4}\,\frac{r^3}{EI_N}\,(F_x \cos\phi - F_z \sin\phi)\cos\phi \\ & + \frac{r^2}{EI_N}\,(M_x \sin\phi + M_z \cos\phi)\cos\phi\end{aligned} \tag{20}$$

$$\begin{aligned}\delta z_p = {} & -\frac{\pi}{4}\,\frac{r^3}{EI_N}\,(F_x \cos\phi - F_z \sin\phi)\sin\phi \\ & + \frac{r^2}{EI_N}\,(M_x \sin\phi + M_z \cos\phi)\sin\phi\end{aligned} \tag{21}$$

---

2. See Ref. 1, Part 1, pp. 7-8.

[redacted]

$$\delta\theta_P = \frac{r^2}{EI_N}\left(F_x \cos\phi - F_z \sin\phi\right)\sin\phi + \frac{\pi}{2}\frac{r}{EI_N}\left(M_x \sin\phi + M_z \cos\phi\right)\sin\phi \tag{22}$$

$$\delta\gamma_P = \frac{r^2}{EI_N}\left(F_x \cos\phi - F_z \sin\phi\right)\cos\phi + \frac{\pi}{2}\frac{r}{EI_N}\left(M_x \sin\phi + M_z \cos\phi\right)\cos\phi \tag{23}$$

Deflections From Out-of-Plane Bending of Channel

The force and moments producing out-of-plane bending of the channel are N, M_P, and M_y. Resolving N and M_P along the coordinate axes,

$$N = F_x \sin\phi + F_z \cos\phi \tag{24}$$

$$M_P = M_z \sin\phi - M_x \cos\phi \tag{25}$$

The deflections due to these loads with respect to the n, p, and y axes are given by[3]

$$\delta n = Nr^3\left[\frac{\pi}{4}\frac{1}{EI_P} + \left(\frac{3\pi}{4} - 2\right)\frac{1}{GK}\right] + \frac{M_P r^2}{2}\left(\frac{1}{EI_P} + \frac{1}{GK}\right) + \frac{M_y r^2}{2}\left[\frac{\pi}{2}\cdot\frac{1}{EI_p} - \frac{1}{GK}\left(2 - \frac{\pi}{2}\right)\right] \tag{26}$$

3. See Ref. 1, Part 2, pp. 13-16.

[redacted]

$$\delta\psi_p = \frac{Nr^2}{2}\left(\frac{1}{EI_p} + \frac{1}{GK}\right) + \frac{\pi}{4} M_p r \left(\frac{1}{EI_p} + \frac{1}{GK}\right) + \frac{M_y r}{2}\left(\frac{1}{EI_p} - \frac{1}{GK}\right) \qquad (27)$$

$$\delta\phi_N = \frac{Nr^2}{2}\left[\frac{\pi}{2}\frac{1}{EI_p} - \left(2 - \frac{\pi}{2}\right)\frac{1}{GK}\right] + \frac{M_p r}{2}\left(\frac{1}{EI_p} - \frac{1}{GK}\right) + \frac{\pi}{4} M_y r \left(\frac{1}{EI_p} + \frac{1}{GK}\right) \qquad (28)$$

Resolving δn and $\delta\psi_p$ into components parallel to the coordinate axes

$$\delta x_N = \delta n \sin\phi \qquad (29)$$

$$\delta z_N = \delta n \cos\phi \qquad (30)$$

$$\delta\gamma_N = \delta\psi_p \sin\phi \qquad (31)$$

$$\delta\theta_N = -\delta\psi_p \cos\phi \qquad (32)$$

Substituting Eqs (24) through (27) into Eqs (28) through (32),

$$\delta\phi_N = \frac{r^2}{2}(F_x \sin\phi + F_z \cos\phi)\left[\frac{\pi}{2}\frac{1}{EI_p} - \left(2 - \frac{\pi}{2}\right)\frac{1}{GK}\right]$$

$$- \frac{r}{2}(M_x \cos\phi - M_z \sin\phi)\left(\frac{1}{EI_p} - \frac{1}{GK}\right) + \frac{\pi}{4} M_y r \left(\frac{1}{EI_p} + \frac{1}{GK}\right) \qquad (33)$$

$$\delta x_N = r^3(F_x \sin\phi + F_z \cos\phi)\left[\frac{\pi}{4}\frac{1}{EI_p} + \left(\frac{3\pi}{4} - 2\right)\frac{1}{GK}\right]\sin\phi$$

$$- \frac{r^2}{2}(M_x \cos\phi - M_z \sin\phi)\left(\frac{1}{EI_p} + \frac{1}{GK}\right)\sin\phi \qquad (34)$$

$$+ \frac{r^2}{2} M_y \left[\frac{\pi}{2}\frac{1}{EI_p} - \left(2 - \frac{\pi}{2}\right)\frac{1}{GK}\right]\sin\phi$$

$$\delta z_N = r^3(F_x \sin\phi + F_z \cos\phi)\left[\frac{\pi}{4}\frac{1}{EI_p} + \left(\frac{3\pi}{4} - 2\right)\frac{1}{GK}\right]\cos\phi$$

$$- \frac{r^2}{2}(M_x \cos\phi - M_z \sin\phi)\left(\frac{1}{EI_p} + \frac{1}{GK}\right)\cos\phi \tag{35}$$

$$+ \frac{r^2}{2} M_y \left[\frac{\pi}{2}\ \frac{1}{EI_p} - \left(2 - \frac{\pi}{2}\right)\frac{1}{GK}\right]\cos\phi$$

$$\delta \gamma_N = \frac{r^2}{2}(F_x \sin\phi + F_z \cos\phi)\left(\frac{1}{EI_p} + \frac{1}{GK}\right)\sin\phi$$

$$- \frac{\pi}{4} r\, (M_x \cos\phi - M_z \sin\phi)\left(\frac{1}{EI_p} + \frac{1}{GK}\right)\sin\phi \tag{36}$$

$$+ \frac{r}{2} M_y \left(\frac{1}{EI_p} - \frac{1}{GK}\right)\sin\phi$$

$$\delta \theta_N = - \frac{r^2}{2}(F_x \sin\phi + F_z \cos\phi)\left(\frac{1}{EI_p} + \frac{1}{GK}\right)\cos\phi$$

$$+ \frac{\pi}{4} r\, (M_x \cos\phi - M_z \sin\phi)\left(\frac{1}{EI_p} + \frac{1}{GK}\right)\cos\phi \tag{37}$$

$$- \frac{r}{2} M_y \left(\frac{1}{EI_p} - \frac{1}{GK}\right)\cos\phi$$

Deflections From Rigid-Body Rotation of Channel About y-axis

The x- and z- deflections from rigid-body rotation of the channel about the y-axis are given by[4]

$$\delta z_r = \overline{ob}\ \delta\phi_r \cos\phi \tag{38}$$

$$\delta x_r = \overline{ob}\ \delta\phi_r \sin\phi \tag{39}$$

Deflections From Deformation of Header Pipe

Since the loads acting on the channel are transmitted to the header pipe in the opposite directions, the deflections of the header pipe may be written in terms of these loads.

$$\delta x_H = -\frac{1}{EI_H}\left(\frac{F_x\ell^3}{3} - \frac{M_y\ell^2}{2}\right) \tag{40}$$

$$\delta\theta_H = -\frac{M_x\ell}{EI_H} \tag{41}$$

$$\delta\phi_H = \frac{1}{EI_H}\left(\frac{F_x\ell^2}{2} - M_y\ell\right) \tag{42}$$

$$\delta\gamma_H = -\frac{M_z\ell}{GJ_H} \tag{43}$$

Solution of Deflection Equations

Substituting Eqs (20)-(23), (33)-(37), (38), (39), and (40)-(43) into Eqs (6)-(11) gives six equations in six unknowns. These can be written in terms of coefficients a_{11}, through a_{16}, as follows:

4. Note that the distance from the origin to b has been denoted by $\overline{ob}$ instead of r. Since the channel is not circular, the actual distances have been used in Eqs (38) and (39) instead of an average radius. The discrepancy involved here is small since $\overline{ob}$ = 24.1 inches and r has been taken as 21.9.

$$
\left.
\begin{array}{l}
a_{11} F_x + a_{12} F_z + a_{13} M_x + a_{14} M_y + a_{15} M_z + a_{16} \phi_r = \delta x_T \\
a_{21} F_x + a_{22} F_z + a_{23} M_x + a_{24} M_y + a_{25} M_z + a_{26} \phi_r = -\delta z_T \\
a_{31} F_x + a_{32} F_z + a_{33} M_x + a_{34} M_y + a_{35} M_z = 0 \\
a_{41} F_x + a_{42} F_z + a_{43} M_x + a_{44} M_y + a_{45} M_z + a_{46} \phi_r = 0 \\
a_{51} F_x + a_{52} F_z + a_{53} M_x + a_{54} M_y + a_{55} M_z = 0 \\
a_{61} F_x + a_{62} F_z + a_{64} M_y = 0
\end{array}
\right\} \quad (44)
$$

where,

$$a_{11} = r^3 \left[\frac{\pi}{4} \frac{1}{EI_P} + \left(\frac{3\pi}{4} - 2\right) \frac{1}{GK}\right] \sin^2\phi + \frac{\pi}{4} \frac{r^3}{EI_N} \cos^2\phi + \frac{\ell^3}{3EI_H}$$

$$a_{12} = r^3 \left[\frac{\pi}{4} \frac{1}{EI_P} + \left(\frac{3\pi}{4} - 2\right) \frac{1}{GK}\right] \sin\phi \cos\phi - \frac{\pi}{4} \frac{r^3}{EI_N} \sin\phi \cos\phi$$

$$a_{13} = -\frac{r^2}{2} \left(\frac{1}{EI_P} + \frac{1}{GK}\right) \sin\phi \cos\phi + \frac{r^2}{EI_N} \sin\phi \cos\phi$$

$$a_{14} = \frac{r^2}{2} \left[\frac{\pi}{2} \frac{1}{EI_P} - \left(2 - \frac{\pi}{2}\right) \frac{1}{GK}\right] \sin\phi - \frac{\ell^2}{2EI_H}$$

$$a_{15} = \frac{r^2}{2} \left(\frac{1}{EI_P} + \frac{1}{GK}\right) \sin^2\phi + \frac{r^2}{EI_N} \cos^2\phi$$

$$a_{16} = \overline{ob} \sin\phi$$

$$a_{21} = r^3 \left[\frac{\pi}{4} \frac{1}{EI_P} + \left(\frac{3\pi}{4} - 2\right) \frac{1}{GK}\right] \sin\phi \cos\phi - \frac{\pi}{4} \frac{r^3}{EI_N} \sin\phi \cos\phi$$

$$a_{22} = r^3 \left[\frac{\pi}{4} \frac{1}{EI_P} + \left(\frac{3\pi}{4} - 2\right) \frac{1}{GK}\right] \cos^2\phi + \frac{\pi}{4} \frac{r^3}{EI_N} \sin^2\phi$$

$$a_{23} = -\frac{r^2}{2}\left(\frac{1}{EI_P} + \frac{1}{GK}\right)\cos^2\phi - \frac{r^2}{EI_N}\sin^2\phi$$

$$a_{24} = \frac{r^2}{2}\left[\frac{\pi}{2}\frac{1}{EI_P} - \left(2 - \frac{\pi}{2}\right)\frac{1}{GK}\right]\cos\phi$$

$$a_{25} = \frac{r^2}{2}\left(\frac{1}{EI_P} + \frac{1}{GK}\right)\sin\phi\cos\phi - \frac{r^2}{EI_N}\sin\phi\cos\phi$$

$$a_{26} = \overline{ob}\cos\phi$$

$$a_{31} = -\frac{r^2}{2}\left(\frac{1}{EI_P} + \frac{1}{GK}\right)\sin\phi\cos\phi + \frac{r^2}{EI_N}\sin\phi\cos\phi$$

$$a_{32} = -\frac{r^2}{2}\left(\frac{1}{EI_P} + \frac{1}{GK}\right)\cos^2\phi - \frac{r^2}{EI_N}\sin^2\phi$$

$$a_{33} = \frac{\pi}{4}r\left(\frac{1}{EI_P} + \frac{1}{GK}\right)\cos^2\phi + \frac{\pi}{2}\frac{r}{EI_N}\sin^2\phi + \frac{\ell}{EI_H}$$

$$a_{34} = -\frac{r}{2}\left(\frac{1}{EI_P} - \frac{1}{GK}\right)\cos\phi$$

$$a_{35} = -\frac{\pi}{4}r\left(\frac{1}{EI_P} + \frac{1}{GK}\right)\sin\phi\cos\phi + \frac{\pi}{2}\frac{r}{EI_N}\sin\phi\cos\phi$$

$$a_{41} = \frac{r^2}{2}\left[\frac{\pi}{2}\frac{1}{EI_P} - \left(2 - \frac{\pi}{2}\right)\frac{1}{GK}\right]\sin\phi - \frac{\ell^2}{2EI_H}$$

$$a_{42} = \frac{r^2}{2}\left[\frac{\pi}{2}\frac{1}{EI_P} - \left(2 - \frac{\pi}{2}\right)\frac{1}{GK}\right]\cos\phi$$

$$a_{43} = -\frac{r}{2}\left(\frac{1}{EI_P} - \frac{1}{GK}\right)\cos\phi$$

$$a_{44} = \frac{\pi}{4} r \left(\frac{1}{EI_P} + \frac{1}{GK}\right) + \frac{\ell}{EI_H}$$

$$a_{45} = \frac{r}{2} \left(\frac{1}{EI_P} - \frac{1}{GK}\right) \sin \phi$$

$$a_{46} = 1$$

$$a_{51} = \frac{r^2}{2} \left(\frac{1}{EI_P} + \frac{1}{GK}\right) \sin^2\phi + \frac{r^2}{EI_N} \cos^2\phi$$

$$a_{52} = \frac{r^2}{2} \left(\frac{1}{EI_P} + \frac{1}{GK}\right) \sin \phi \cos \phi - \frac{r^2}{EI_N} \sin \phi \cos \phi$$

$$a_{53} = - \frac{\pi}{4} r \left(\frac{1}{EI_P} + \frac{1}{GK}\right) \sin \phi \cos \phi + \frac{\pi}{2} \frac{r}{EI_N} \sin \phi \cos \phi$$

$$a_{54} = \frac{r}{2} \left(\frac{1}{EI_P} - \frac{1}{GK}\right) \sin \phi$$

$$a_{55} = \frac{\pi}{4} r \left(\frac{1}{EI_P} + \frac{1}{GK}\right) \sin^2\phi + \frac{\pi}{2} \frac{r}{EI_N} \cos^2\phi + \frac{\ell}{GJ_H}$$

$$a_{61} = z_b$$

$$a_{62} = - x_b$$

$$a_{64} = 1$$

Results

Equations (44) were solved with the aid of an IBM-650. The numerical data and values of the coefficients are given in Appendix A. The following results were obtained:

$$
\left.
\begin{aligned}
F_x &= 565.9 \text{ lbs.} \\
F_z &= -426.7 \text{ lbs.} \\
M_x &= -5462 \text{ in-lbs.} \\
M_y &= 391 \text{ in-lbs.} \\
M_z &= -6620 \text{ in-lbs.} \\
\phi_r &= -3.468 \times 10^{-3} \text{ radian}
\end{aligned}
\right\} \qquad (45)
$$

Calculation of Deflections

The y-deflection at b relative to point a can be calculated from the loads producing in-plane bending[5].

$$\delta y = \frac{Pr^3}{2EI_N} - \left(\frac{\pi}{2} - 1\right) \frac{M_N r^2}{EI_N} \qquad (46)$$

Substituting P and M_N from Eqs (12) and (13) into Eq (46),

$$\delta y = -\frac{r^3}{2EI_N} (F_x \cos\phi - F_z \sin\phi) - \left(\frac{\pi}{2} - 1\right) \frac{r^2}{EI_N} (M_x \sin\phi + M_z \cos\phi) \qquad (47)$$

---

5. See Ref. 1, pp. 7-8.

Using the values (45) for the forces and moments in Eq (47),

$$\delta y = -0.0373 \text{ in.}$$

This result indicates that the channel will expand 37 mils towards Shell V, at the equator, in addition to the free relative thermal expansion reported in ART Design Memo 8-D-5.

Since there are no forces on the channel in the y-direction, the y-deflection at b, relative to the actual coordinate system, is zero.

The x-deflection at b can be calculated by summing the in-plane and out-of-plane x-deflections for the channel, or from the deflection of the header pipe. Taking the latter, and using Eq (40),

$$\delta x = -\frac{1}{EI_H}\left(\frac{F_x \ell^3}{3} - \frac{M_y \ell^2}{2}\right) = -0.00299 \text{ in.}$$

The angular deflections at b can be calculated from the deformation of the header pipe, using Eqs (41), (42), and (43).

$$\delta \theta = -\frac{M_x \ell}{EI_H} = 1.785 \times 10^{-3} \text{ rad.}$$

$$\delta \phi = \frac{1}{EI_H}\left(\frac{F_x \ell^2}{2} - M_y \ell\right) = 5.657 \times 10^{-4} \text{ rad.}$$

$$\delta \gamma = -\frac{M_z \ell}{GJ_H} = 2.813 \times 10^{-3} \text{ rad.}$$

Stresses in Channel at Header

The stresses in the channel at point b (Fig. 2) can be calculated from the moments, M_N M_P, and M_y. From Eqs (12), (13), (24), and (25), with the values from (45),

$$P = F_z \sin \phi - F_x \cos \phi = -708.5 \text{ lbs.}$$

$$M_N = M_x \sin \phi + M_z \cos \phi = -8563 \text{ in-lbs.}$$

$$N = F_x \sin \phi + F_z \cos \phi = + 16.22 \text{ lbs.}$$

$$M_P = M_z \sin \phi - M_x \cos \phi = 572 \text{ in-lbs.}$$

The maximum bending stresses due to M_N and M_P are calculated as follows:

$$\sigma_P = \pm \frac{M_P}{z_P} = \pm 83 \text{ psi}$$

$$\sigma_N = -\frac{M_N}{z_N} = 8234 \text{ psi}$$

The maximum shear stress due to M_y may be estimated by an approximate method[6]. This stress occurs at or near the inside corner of the channel. (See Fig. 4)

$$\tau_{max} = \frac{M_y C}{K} \tag{48}$$

where

K = a function of the cross section of the channel used in calculating the torsional rigidity[7]

$= 0.09295 \text{ in}^4$

$$C = \frac{D}{1 + \frac{\pi^2 D^4}{16A^2}} \left\{ 1 + \left[0.118 \ln \left(1 - \frac{D}{2r} \right) - 0.238 \frac{D}{2r} \right] \tan h \frac{2\phi}{\pi} \right\} \tag{49}$$

6. See Ref. 2, pp. 170-181.

7. The evaluation of K is given in Appendix B.

[redacted]

where

D = diameter of the largest circle inscribed in the cross section = 0.45 in.

r = radius of curvature of the boundary at the point (negative when Eq 49 is used) = - 0.110 in.

A = area of the section = 2.582 in^2

ϕ = angle through which a tangent to the boundary rotates in turning or traveling around the reentrant portion, measured in radians = $\pi/2$

For these values,

C = 0.8612 in.

Using Eq (48) with the above values of C and K,

$$\tau_{max} = 3623 \text{ psi}$$

Stresses in Channel at Equator

The moments tangent, radial, and normal to the curve at the equator may be expressed from equilibrium conditions, (see Figs. 3 and 5).

$$M_t = M_P + Nr = 217.2 \text{ in-lbs.}$$

$$M_r = - M_y = - 391 \text{ in-lbs.}$$

$$M_n = - M_N + Pr = - 6954 \text{ in-lbs.}$$

The maximum bending stresses due to M_r and M_n given by

$$\sigma_r = \pm \frac{M_r}{z_P} = \pm 57 \text{ psi}$$

$$\sigma_n = \frac{M_n}{z_N} = - 6687 \text{ psi}$$

[redacted]

[redacted]

[redacted]

ORNL-LR-DWG. 27497

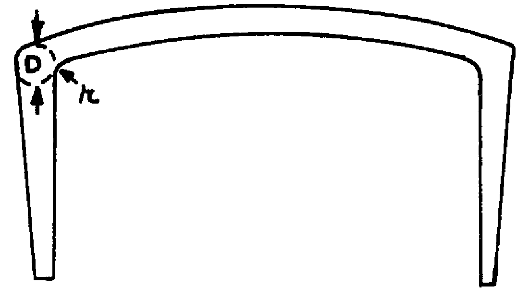

FIG. 4 – CROSS-SECTION OF CHANNEL

[redacted]

ORNL-LR-DWG. 27498

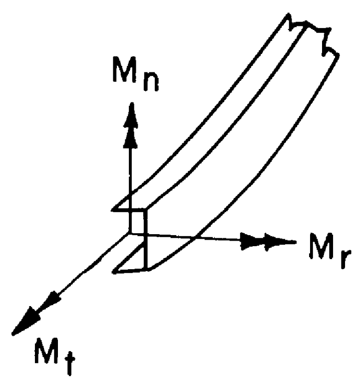

FIG. 5 – SKETCH SHOWING PRINCIPAL MOMENTS
ON CHANNEL AT EQUATOR

[redacted]

[redacted]

The maximum shear stress due to M_t can be calculated by Eq (48). Using the same C/K ratio as before,

$$\tau_{max} = 2013 \text{ psi} \quad .$$

Stresses in Header Pipe

Bending stresses are produced in the header pipe from F_x, M_x and M_y. Referring to Fig. 3 the moment in the y-direction at the fixed end of the pipe due to F_x and M_y is given by

$$M_{Hy} = M_y - F_x \ell = -3853 \text{ in-lbs.}$$

The moment in the x-direction at the fixed end is

$$M_{Hx} = M_x = -5462 \text{ in-lbs.}$$

Taking the vector sum of these moments gives a maximum bending moment,

$$M_H = -6684 \text{ in-lbs.}$$

The maximum bending stress due to this moment is given by

$$\sigma_H = \pm \frac{M_H}{z_H} = \pm 6282 \text{ psi} \quad .$$

The maximum shear stress due to M_z is given by

$$\tau_{max} = \frac{M_z r_H}{J_H} = -3111 \text{ psi} \quad .$$

[redacted]

[redacted]

Thermal stresses are produced in the header pipe from radial and axial temperature gradients, in addition to those caused by relative thermal expansion of the channel. Figure 6 shows the north and south headers and pipes with the approximate temperatures of the surrounding fluids.

The axial temperature gradients should be small except in the regions close to the headers which are subjected to cross-flow from the fuel. Because of the azimuthal variation in heat transfer coefficients and the complicated geometry of these regions, it is possible that thermal cycling of these small sections of pipe could occur. Although these temperature fluctuations would be difficult to calculate, small thermal shields welded to the headers might be warranted.

Because the layer of fuel surrounding the header pipes over most of their lengths is very thin, an estimate of the radial temperature profiles may be calculated using simple conduction with semi-infinite slab geometry. With the temperatures indicated in Fig. 6, these calculations give temperature differences across the walls of 23°F and 32°F for the north and south header pipes, respectively. The stresses in the outside walls due to these gradients can be calculated by

$$\sigma = \frac{\alpha E \Delta T}{1 - \nu} , \qquad (43)$$

giving - 4574 psi for the north header pipe, and 6176 psi for the south.

The bending and twisting stresses may now be combined with the stresses due to the radial temperature gradient in the header pipe in order to get the maximum normal and shear stresses. Figure 7 shows the fixed end of the header pipe, the direction of the resultant bending moment, and the bending stresses due to M_H. Since the twisting stresses

[redacted]

[redacted]

[redacted]
ORNL-LR-DWG. 27499

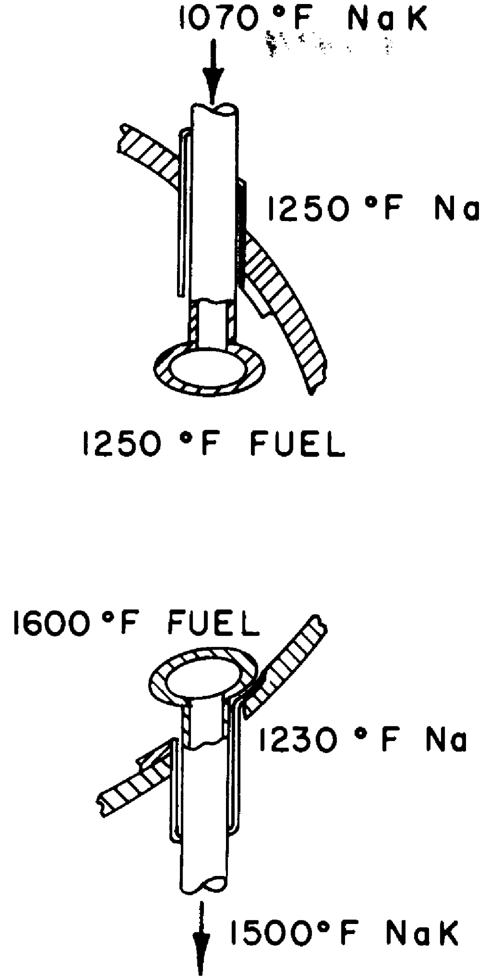

FIG. 6 - SKETCH SHOWING NORTH AND SOUTH HEADER PIPES APPROXIMATE FLUID TEMPERATURES

ORNL-[redacted] 27500

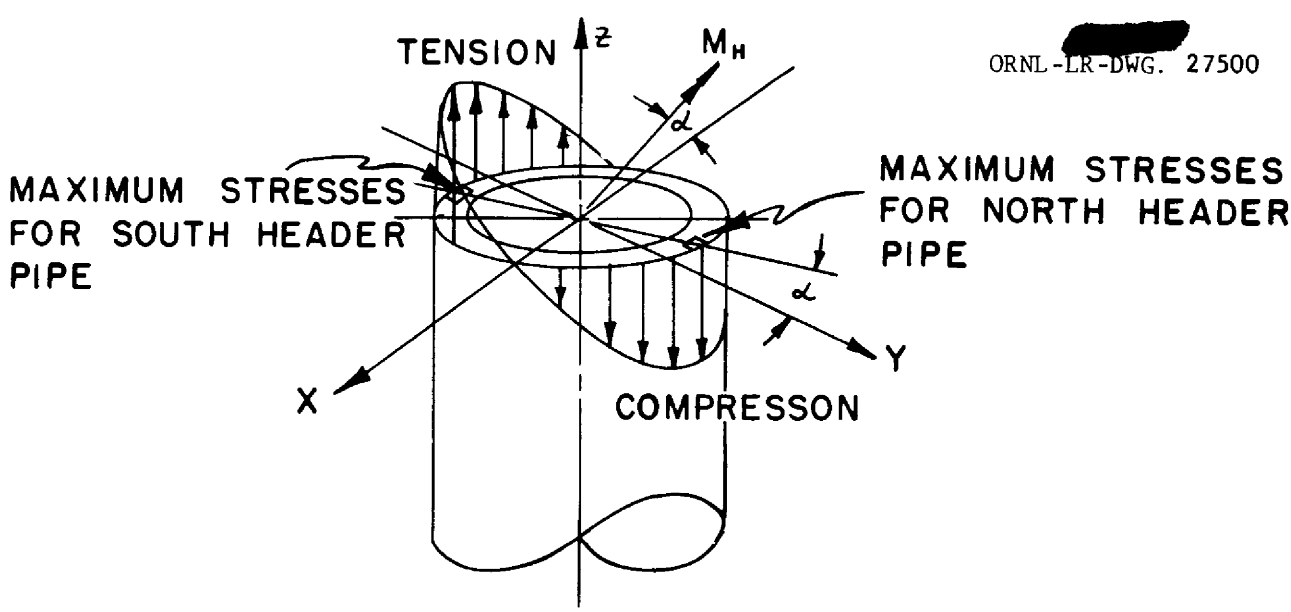

FIG. 7 - FIXED END OF HEADER PIPE SHOWING BENDING STRESSES AND ELEMENTS AT WHICH MAXIMUM STRESSES OCCUR

[redacted]

and temperature gradient stresses are uniformly distributed around the header pipe, the direction of M_H determines the location of the maximum stresses in the pipe. For the north header pipe, the temperature gradient stresses are compressive at the outside wall, so the maximum stresses occur where the bending stress is a maximum in compression. This element is at the outside wall, 90° clockwise from the direction of $- M_H$ and an angle α counterclockwise from the positive y-axis, where

$$\alpha = \tan^{-1}\left(\frac{M_{yH}}{M_{xH}}\right) = 35.2^{\circ}$$

For the south header, the temperature gradient stresses are tensile at the outer wall, so the maximum stresses occur where the bending stress is a maximum in tension. This point is 180° from the point of maximum stress in the north header pipe, or an angle α counter clockwise from the negative y-axis, when the south header pipe is oriented as in Fig. 7 (eg the z-axis is directed away from the equator).

The maximum stresses can be calculated for the north and south header pipes from the combined stresses acting on the elements in the outer walls of the header pipes, as shown in Fig. 7. The stresses acting on these elements are shown in Fig. 8. The maximum normal and shear stresses are given by

$$\sigma_{max} = \frac{1}{2}(\sigma_1 + \sigma_2) \pm \left[\left(\frac{\sigma_1 - \sigma_2}{2}\right)^2 + \tau^2\right]^{1/2} \qquad (44)$$

$$\tau_{max} = \left[\left(\frac{\sigma_1 - \sigma_2}{2}\right)^2 + \tau^2\right]^{1/2} \qquad (45)$$

[redacted]

[redacted]

[redacted]

ORNL-LR-DWG. 27501

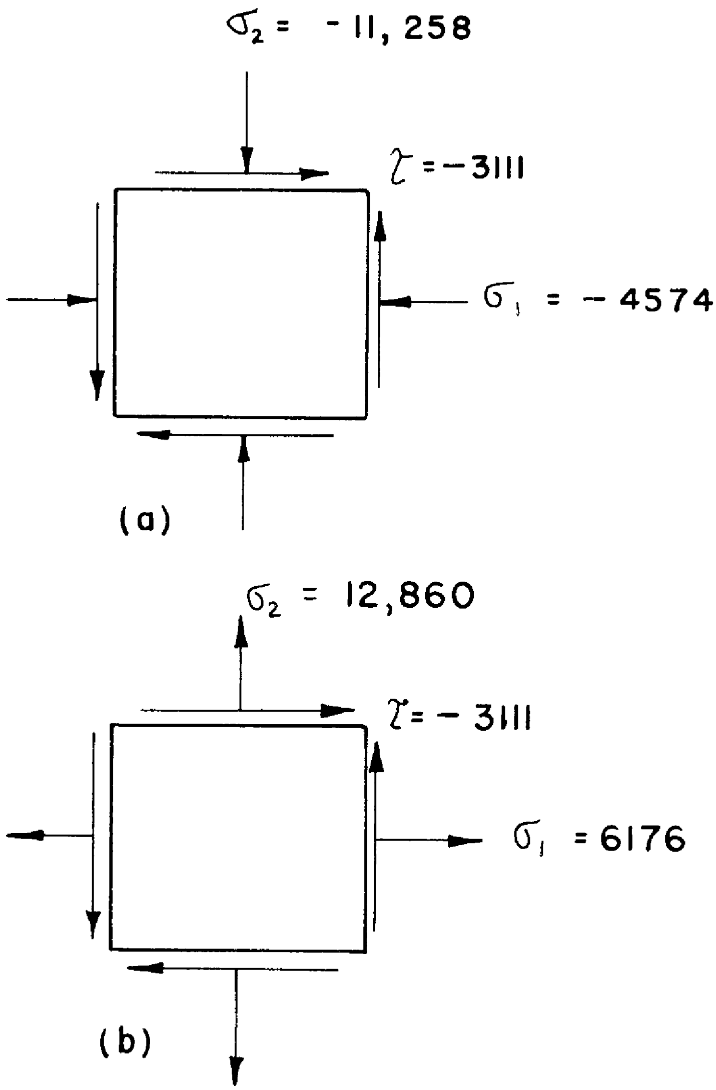

FIG. 8 – ELEMENTS UNDER MAXIMUM STRESS IN OUTSIDE WALL OF (a) NORTH HEADER PIPE; (b) SOUTH HEADER PIPE (STRESSES IN psi)

[redacted]

For the north header pipe,

$$\sigma_{max} = -12{,}480 \text{ psi}$$

$$\tau_{max} = 4565 \text{ psi.}$$

For the south header pipe,

$$\sigma_{max} = 14{,}080 \text{ psi}$$

$$\tau_{max} = 4565 \text{ psi.}$$

References

1. D. L. Platus and B. L. Greenstreet, "Deflection Equations for Various Loadings of Circular-Arc Curved Beams", CF 57-4-96.

2. R. J. Roark, <u>Formulas for Stresses and Strain</u>, Third Edition, 1954, pp 170-181.

3. S. Timoshenko and J. N. Goodier, <u>Theory of Elasticity</u>, Second Edition, 1951, p. 287.

4. S. Timoshenko, <u>Strength of Materials</u>, Part II, 1941, pp 270-271.

Appendix A

Numerical Data

x_b	=	- 19.59 in.	
z_b	=	14.08 in.	
r	=	21.9 in.	
$\overline{ob}$	=	24.125 in.	
ℓ	=	7.50 in.	
E	=	15×10^6 psi	
ν	=	0.3	
G	=	5.8×10^6 psi	
I_P	=	20.72 in^4	
I_N	=	2.46 in^4	
K	=	0.09295 in^4	
I_H	=	1.53 in^4	2-1/2 inch Sch 40 Pipe
J_H	=	3.06 in^4	2-1/2 inch Sch 40 Pipe
δx_T	=	0.032 in.	
δz_T	=	0.041 in.	

Numerical Values of Coefficients Used in Eqs (44)

a_{11}	=	2538.7×10^{-6}	a_{21}	=	3212.6×10^{-6}
a_{12}	=	3212.9×10^{-6}	a_{22}	=	4693.5×10^{-6}
a_{13}	=	-206.19×10^{-6}	a_{23}	=	-299.76×10^{-6}
a_{14}	=	-112.53×10^{-6}	a_{24}	=	-154.86×10^{-6}
a_{15}	=	161.18×10^{-6}	a_{25}	=	206.19×10^{-6}
a_{16}	=	14.079	a_{26}	=	19.59

a_{31}	=	-206.19×10^{-6}
a_{32}	=	-299.88×10^{-6}
a_{33}	=	21.173×10^{-6}
a_{34}	=	16.55×10^{-6}
a_{35}	=	-14.787×10^{-6}

[redacted]

$a_{41} = -\,112.53\text{x}10^{-6}$

$a_{42} = -\,154.88\text{x}10^{-6}$

$a_{43} = 16.55\text{x}10^{-6}$

$a_{44} = 32.464\text{x}10^{-6}$

$a_{45} = -\,11.896\text{x}10^{-6}$

$a_{46} = 1.0000$

$a_{51} = 161.18\text{x}10^{-6}$

$a_{52} = 206.17\text{x}10^{-6}$

$a_{53} = -\,14.787\text{x}10^{-6}$

$a_{54} = -\,11.896\text{x}10^{-6}$

$a_{55} = 11.986\text{x}10^{-6}$

$a_{61} = 14.08$

$a_{62} = 19.59$

$a_{64} = 1.0000$

[redacted]

[redacted]

Appendix B

Evaluation of Torsional Rigidity Factor, K

For a narrow rectangular beam of length b and width c, K can be approximated using the membrane analogy to give[8]

$$K = \frac{1}{3} bc^2 \qquad \text{(B1)}$$

Similarly, for a narrow trapezoidal section[9],

$$K = \frac{1}{12} b_1(c_1 + c_2)(c_1^2 + c_2^2) \qquad \text{(B2)}$$

For a cross-section built up of narrow elements, K can be approximated by summing the K's for the individual elements[10]. Thus, for the channel (Fig. 4), by summing two trapezoidal sections and one rectangle,

$$K = \frac{1}{3} bc^3 + \frac{1}{6} b_1(c_1 + c_2)(c_1^2 + c_2^2) \qquad \text{(B3)}$$

---

8. See Ref. 4, p. 270.
9. See Ref. 4, p. 271.
10. See Ref. 3, p. 287.

[redacted]

Using Eq (B3) with

$b = 5.00$ in.

$c = 0.125$ in.

$b_1 = 3.45$ in.

$c_1 = 0.10$ in.

$c_2 = 0.50$ in.

$K = 0.09295 \text{ in}^4$

[redacted]

ORNL-2442
C-84 - Reactors - Special Features of Aircraft Reactors
M-3679 (20th ed., Rev.)

INTERNAL DISTRIBUTION

1. J. C. Amos
2. D. S. Billington
3. F. F. Blankenship
4. E. P. Blizard
5. A. L. Boch
6. C. J. Borkowski
7. G. E. Boyd
8. E. J. Breeding
9. R. B. Briggs
10. D. W. Cardwell
11. C. E. Center (K-25)
12. R. A. Charpie
13. B. Y. Cotton
14. F. L. Culler
15. J. H. DeVan
16. D. A. Douglas
17. L. B. Emlet (K-25)
18. D. E. Ferguson
19. A. P. Fraas
20. J. H. Frye, Jr.
21. W. T. Furgerson
22. R. J. Gray
23. B. L. Greenstreet
24. W. R. Grimes
25. E. Guth
26. C. S. Harrill
27. R. L. Heestand
28. H. W. Hoffman
29. A. Hollaender
30. A. S. Householder
31. W. H. Jordan
32. P. R. Kasten
33. G. W. Keilholtz
34. M. T. Kelley
35. J. L. Kerrebrock
36. J. A. Lane
37. R. S. Livingston
38. H. G. MacPherson
39. R. E. MacPherson
40. W. D. Manly
41. J. R. McNally
42. R. V. Meghreblian
43. K. Z. Morgan
44. E. J. Murphy
45. J. P. Murray (Y-12)
46. M. L. Nelson
47. P. Patriarca
48. A. M. Perry
49. H. W. Savage
50. A. W. Savolainen
51. R. D. Schultheiss
52. R. L. Senn
53. E. D. Shipley
54. M. J. Skinner
55. A. H. Snell
56. F. J. Stanek
57. J. A. Swartout
58. A. Taboada
59. J. R. Tallackson
60. E. H. Taylor
61. D. B. Trauger
62. A. M. Weinberg
63. C. E. Winters
64. M. M. Yarosh

65-67. ORNL - Y-12 Technical Library, Document Reference Section
68-75. Laboratory Records Department
76. Laboratory Records ORNL R.C.
77-79. Central Research Library
80. Reactor Experimental Engineering Library

EXTERNAL DISTRIBUTION

81. Division of Research and Development, AEC, ORO
82-84. Air Force Ballistic Missile Division
85-86. AFPR, Boeing, Seattle
87. AFPR, Boeing, Wichita
88. AFPR, Curtiss-Wright, Clifton
89. AFPR, Douglas, Long Beach
90-92. AFPR, Douglas, Santa Monica

[redacted]

[redacted]

93. AFPR, Lockheed, Burbank
94-95. AFPR, Lockheed, Marietta
96. AFPR, North American, Canoga Park
97. AFPR, North American, Downey
98-99. Air Force Special Weapons Center
100. Air Materiel Command
101. Air Research and Development Command (RDGN)
102. Air Research and Development Command (RDTAPS)
103-116. Air Research and Development Command (RDZPSP)
117. Air Technical Intelligence Center
118-120. ANP Project Office, Convair, Fort Worth
121. Albuquerque Operations Office
122. Argonne National Laboratory
123. Armed Forces Special Weapons Project, Sandia
124. Armed Forces Special Weapons Project, Washington
125. Assistant Secretary of the Air Force, R&D
126-131. Atomic Energy Commission, Washington
132. Atomics International
133. Battelle Memorial Institute
134-135. Bettis Plant (WAPD)
136. Bureau of Aeronautics
137. Bureau of Aeronautics General Representative
138. BAR, Aerojet-General, Azusa
139. BAR, Convair, San Diego
140. BAR, Glenn L. Martin, Baltimore
141. BAR, Grumman Aircraft, Bethpage
142. Bureau of Yards and Docks
143. Chicago Operations Office
144. Chicago Patent Group
145. Curtiss-Wright Corporation
146. Engineer Research and Development Laboratories
147-150. General Electric Company (ANPD)
151. General Nuclear Engineering Corporation
152. Hartford Area Office
153. Idaho Operations Office
154. Knolls Atomic Power Laboratory
155. Lockland Area Office
156. Los Alamos Scientific Laboratory
157. Marquardt Aircraft Company
158. Martin Company
159. National Advisory Committee for Aeronautics, Cleveland

[redacted]

[redacted]

160. National Advisory Committee for Aeronautics, Washington
161. Naval Air Development Center
162. Naval Air Material Center
163. Naval Air Turbine Test Station
164. Naval Research Laboratory
165. New York Operations Office
166. Nuclear Development Corporation of America
167. Nuclear Metals, Inc.
168. Office of Naval Research
169. Office of the Chief of Naval Operations (OP-361)
170. Patent Branch, Washington
171-174. Pratt and Whitney Aircraft Division
175. San Francisco Operations Office
176. Sandia Corporation
177. School of Aviation Medicine
178. Sylvania-Corning Nuclear Corporation
179. Technical Research Group
180. USAF Headquarters
181. USAF Project RAND
182. U.S. Naval Radiological Defense Laboratory
183-184. University of California Radiation Laboratory, Livermore
185-202. Wright Air Development Center (WCOSI-3)
203-227. Technical Information Service Extension, Oak Ridge

[redacted]